

## Article

# Hydroclimate Changes Based on Testate Amoebae in the Greater Khingan Mountains' Peatland (NE China) during the Last Millennium

Xiao Li <sup>1,2,3</sup>, Dongxue Han <sup>1,2</sup>, Jinxin Cong <sup>1,2</sup>, Chuanyu Gao <sup>1,2,\*</sup>  and Guoping Wang <sup>1,2,\*</sup> 

- <sup>1</sup> State Key Laboratory of Black Soils Conservation and Utilization, Northeast Institute of Geography and Agroecology, Chinese Academy of Sciences, Changchun 130102, China; lixiao@iga.ac.cn (X.L.)
- <sup>2</sup> Key Laboratory of Wetland Ecology and Environment, Northeast Institute of Geography and Agroecology, Chinese Academy of Sciences, Changchun 130102, China
- <sup>3</sup> University of Chinese Academy of Sciences, Beijing 100049, China
- \* Correspondence: gaochuanyu@iga.ac.cn (C.G.); wangguoping@iga.ac.cn (G.W.)

**Abstract:** The driving force of climate change in the monsoon margin is complex, making it a key area for regional and global climate change research. Palaeohydrological studies in the monsoon margin have increased the resolution of research in the long term, transitioning from qualitative to quantitative studies to comprehend climate change processes, patterns, and mechanisms. Testate amoebae (TA) in peat sediments are used as a proxy indicator organism for quantitative reconstruction of palaeohydrology. Thus, their community changes are directly related to precipitation, and widely used to reconstruct the patterns of summer precipitation globally. We investigated TA species and reconstructed palaeohydrological changes in the Greater Khingan Mountains' Hongtu (HT) peatland, located in the East Asian Summer Monsoon (EASM) margin. The result showed that the most abundant TA species were *Assulina muscorum* ( $12.4 \pm 5.0\%$ ) and *Nebela tinctoria* ( $8.9 \pm 4.9\%$ ) in the HT peat core. The increase in dry indicator species (e.g., *A. muscorum* and *Alabasta militaris*) indicated a drying pattern in the HT peatland since 150 cal yr BP. Principal component analysis (PCA) explained 47.6% of the variation in the selected TA assemblages. During 400 to 250 cal yr BP, PCA axis 1 scores ranged from 0.2 to  $-1.3$  (reflecting a drier climate), associating with the Little Ice Age. The paleohydrology of the northern part of the Greater Khingan Mountains was mainly controlled by the EASM, which was associated with changes in North Atlantic Sea surface temperature and solar radiative forcing. The apparent drying pattern may be the result of the gradual intensification of anthropogenic activities and the increase in EASM intensity.

**Keywords:** peatland; testate amoebae; East Asian Summer Monsoon; reconstruction; palaeohydrology



**Citation:** Li, X.; Han, D.; Cong, J.; Gao, C.; Wang, G. Hydroclimate Changes Based on Testate Amoebae in the Greater Khingan Mountains' Peatland (NE China) during the Last Millennium. *Atmosphere* **2024**, *15*, 314. <https://doi.org/10.3390/atmos15030314>

Academic Editors: Davide Zanchettin and Gianni Bellocchi

Received: 10 January 2024  
Revised: 27 February 2024  
Accepted: 27 February 2024  
Published: 1 March 2024



**Copyright:** © 2024 by the authors. Licensee MDPI, Basel, Switzerland. This article is an open access article distributed under the terms and conditions of the Creative Commons Attribution (CC BY) license (<https://creativecommons.org/licenses/by/4.0/>).

## 1. Introduction

The global climate system is significantly influenced by the East Asian Summer Monsoon (EASM) and westerlies [1]. The EASM, due to differences in thermal properties between land and sea, dominates precipitation in southern and eastern China and is a key factor in the formation and propagation of summer rain belts [2,3]. The westerlies influence precipitation in western and northern China by transporting water vapor from the North Atlantic and lakes or inland seas along their path [3]. The northeastern region of China is influenced by both the EASM and westerlies due to its location at the monsoon margin, making it susceptible to regional and global climate changes [4]. The complexity of the driving forces behind climate change in this area makes it a key focus for regional and global climate change research.

Climate change over the past millennium has been the result of a combination of the natural environment and human activities [5,6]. For example, climate change has led to significant spatial and temporal differences in precipitation patterns in summer

wind-affected regions of East Asia. These variations have resulted in a reduction in tree species and wetland areas in China, as well as an increase in the frequency of extreme weather events [7–9]. Based on instrumental observations in recent decades, there is a clear south–north dipole pattern of precipitation in the eastern monsoon region of China [10,11], and palaeoclimate reconstructions suggest that this climate pattern also existed in the late Holocene and even longer time scales [11–13]. Taking the Summer Monsoon Limit as the east–west boundary, the dry–wet pattern in the eastern monsoon region of China during the Medieval Warm Period and the Little Ice Age (during the period of global cooling from 1300 to 1850 AD) has a south–north dipole pattern, i.e., the southeastern part of the region is characterized by a dry Medieval Warm Period drought and a wet Little Ice Age climate (i.e., warm/dry—cold/wet), while the northern part is the opposite (warm/wet—cold/dry). However, there are studies suggesting a warm/wet–cold/dry climate in the southern part of the eastern monsoon region and a warm/dry–cold/wet climate in the northern part, such as the reconstructions of Dongge Cave in Guizhou [12] and Dali Lake in Inner Mongolia [14]. Therefore, more high-resolution millennial hydrological reconstructions from the eastern monsoon region, especially from the monsoon margins, are still urgently needed to better understand the complex climate change patterns and their underlying driving mechanisms in the EASM over the past millennia to more accurately predict and respond to future climate change.

Peat sediments are widely used in palaeohydrological and palaeoclimate reconstruction studies due to their high resolution, continuity, and ability to record a wealth of environmental information [15]. Peat archives that indicate palaeohydrological changes, such as humification, macrofossil plants, and testate amoebae (Protozoa: Rhizopoda; TA), are important parameters for palaeoclimate studies [16–19]. TA are widely distributed in peatlands [20,21]. Recent ecological studies have shown that the community structure and diversity of TA in peatlands are mainly regulated by soil moisture, water table depth (WTD), and hydrochemistry [22–25]. Different species of TA show different and relatively narrow ecological spokes to environmental factors, and their shells have good corrosion resistance, are well preserved in peat deposits, are easy to extract, and have stable morphology [20]. And their morphological characteristics can identify the species, making them an effective paleoenvironmental indicator organism [25–28]. Therefore, fossil TA are also used as proxy indicator organisms for quantitative reconstruction of palaeohydrology (WTD, soil moisture, and hydrochemistry), and their community changes are directly related to climate indicators such as precipitation [1,29,30].

Principal Component Analysis (PCA) is a widely utilized mathematical dimension reduction method. PCA transforms a series of potentially linearly correlated variables into a set of linearly uncorrelated new variables, also known as principal components, through orthogonal transformation. This allows us to extract the main patterns from a large volume of species data, thereby simplifying calculations and resultant interpretations. A multitude of studies have demonstrated that PCA analysis utilizing species data can be employed to delineate habitat characteristics, contrast habitat differences, and investigate the primary habitat indicators [13,31–33]. Transfer functions, commonly used for quantitatively reconstructing water levels, pH, and humidity [34–36], do indeed have inherent limitations. Notably, the precision of a transfer function heavily relies on the quality of the original data. Additionally, the transfer function relies on instantaneous measurements of groundwater levels rather than annual averages, significantly impacting its accuracy. Furthermore, different species of TA (testate amoebae) may exhibit varying responses to environmental changes [37]. In complex environments where multiple environmental factors concurrently influence TA distribution, establishing and applying the transfer function can indeed become intricate [21].

The Greater Khingan Mountains, located on the northern margin of the EASM and the southern edge of the global boreal permafrost zone, are mainly influenced by both the EASM and westerlies [38], and belong to the temperate continental monsoon climate or temperate monsoon climate [39,40]. With climate change and human activity increased,

disturbance events such as fires have led to permafrost degradation and hydrological changes in the region [41]. Several studies have used peat cellulose,  $^{13}\text{C}$  values of n-alkanes, black carbon, and pollen in peat sequences to reconstruct the climatic characteristics of the Greater Khingan Mountains [5,13,38,41,42]. However, there are few palaeohydrological studies of the region, and the hydrology of the past millennium is unclear. As this region is located at the EASM margin and the westerlies' local climate forcing mechanism is complex and variable, comparative studies on the palaeohydrological and paleoclimate of this region should be strengthened.

In the present study, we investigated high-resolution TA records from the Hongtu (HT) peatland in the Greater Khingan Mountains in the past millennium. The TA communities and paleohydrology were reconstructed using TA records, accelerator mass spectrometry (AMS)  $^{14}\text{C}$  dating, and PCA. The palaeohydrological record was compared with other paleoclimate records in the EASM to explore possible driving mechanisms of climate change. Our study subjective aims included the following: 1. To analyze the changes in TA community structure during the millennium. 2. To verify historical patterns in TA and their environmental implications. 3. To explore the driving mechanism of peatland paleohydrology.

## 2. Materials and Methods

### 2.1. Study Area and Sampling

The peatland under study is situated in the northern Greater Khingan Mountains of northeastern China (Figure 1). The Greater Khingan Mountains have an elevation range of 180–2029 m above sea level. The mountains experience dry, cold winters from November to April and wet, hot summers from July to August [13]. The Greater Khingan Mountains have a temperate continental monsoon climate with an average annual temperature of  $-2.8\text{ }^{\circ}\text{C}$  and an average annual precipitation of 460–520 mm [43,44]. The dominant vegetation species of the HT peatland were *Vaccinium uliginosum*, *Ass. Ledum palustre var. angustum*, *Carex schmidtii*, and *Alnus hirsute*. The HT peat bog ( $51.62^{\circ}\text{ N}$ ,  $124.24^{\circ}\text{ E}$ , altitude 550 m) is located in a valley, and the presence of several mountain peaks (elevations higher than 1000 m) is influenced by the EASM and the westerlies.

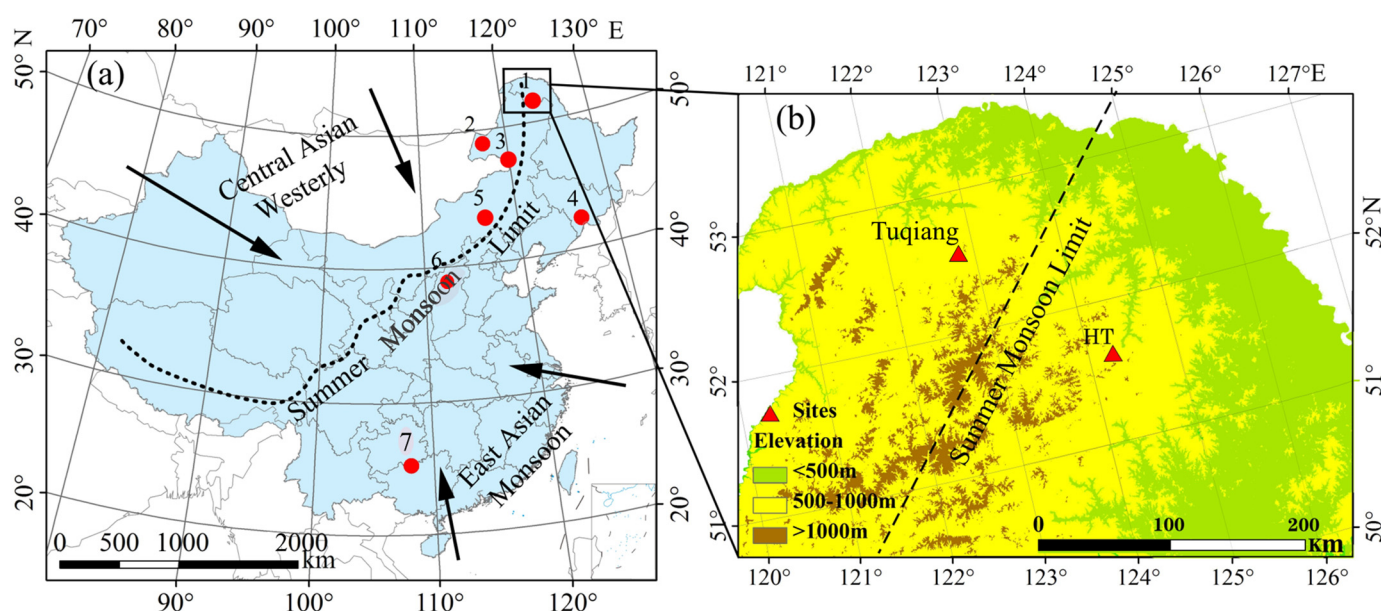


**Figure 1.** (a) Locations of the HT peatland in the Greater Khingan Mountains and other sites discussed in this study. 1. HT peatland [38] and Tuqiang peatland [45]; 2. Hulun Lake [5]; 3. Motianling peatland [42]; 4. Sihailongwan Maar Lake [46]; 5. Dali Lake [14]; 6. Gonghai Lake [47]; 7. Dongge Cave [12]. (b) Locations of the HT and Tuqiang peatlands in the Greater Khingan Mountains (red triangles). The dashed line is the Summer Monsoon Limit [48].

The HT core (depth 60 cm) was collected in the mountains in September 2014. Surface samples were collected from a dug profile and bottom samples were collected using a 500 × 50 mm Russian corer. The location was determined using a GPS (ICEGPS 110/610) unit. The core was cut at 1 cm intervals for analysis and samples were stored in plastic bags. Detailed  $^{14}\text{C}$  dating results are presented in the published article [38].

## 2.2. Chronology

We obtained three radiocarbon dates from the HT core. The bulk sediments were prepared according to the protocol detailed in Zhou, Lu, Wu, Deng, Jull, and Beck [49], and the analyses were conducted at the accelerator mass spectrometry (AMS) facility in Xi'an. The  $^{14}\text{C}$  dates were converted to calibrated ages (cal yr BP) using the CALIB software package, version 7.04, which relies on the 2013 international calibration datasets [50]. Table 1 provides further information, and the detail age-depth model, which quantifies the total chronological error and returns the maximum age probabilities at 1 cm intervals, were shown in our previous published article [38].

**Table 1.** Radiocarbon ages and calibrate age data for the HT peat sequences [38].

Depth (cm)	Laboratory Code <sup>a</sup>	Dated Material	$^{14}\text{C}$ yr BP	Calibrated Age
19	XA12145	Bulk peat	175 ± 30	135–225
39	XA12146	Bulk peat	328 ± 25	308–465
59	XA12147	Bulk peat	866 ± 28	700–801

<sup>a</sup> XA, Xi'an Institute of Earth Environment, Chinese Academy of Sciences.

## 2.3. Testate Amoebae Analysis

TA samples were prepared using the methods of Charman, D and W.A [51] and Booth, M and Charman [26]. The procedure for preparing samples for TA identification involved a method that included water suspension, physical shaking, and subsequent settling. Initially, two grams of the substrate was immersed in distilled water for 24 h, followed by a 10 min agitation on a flask shaker. The samples were then sieved and rinsed through 300 µm and 0.5 µm mesh to eliminate larger particles and allowed to settle for another 24 h. The remaining fraction was washed into a tube and centrifuged. The supernatant was then carefully removed to reduce the sample volume to 10 mL. These samples were combined with neutralized formaldehyde and stored in glass vials. A droplet of the concentrated sample was placed on a microscope (Olympus BX-53, Olympus Corporation, Tokyo, Japan) slide, blended with glycerol, and examined under 200–400× magnification. All TA encountered were identified using a morphology-based approach and tallied as per identification guides, aiming for 150 tests per sample [20,52].

The TA taxonomic scheme developed by Charman [20] and Charman, D and W.A [51] has been widely used in recent TA ecological studies [34,53,54]. We assigned *Phryganella acropodia*, *P. acropodia penardi*, and *P. hemisphaerica* to the *Phryganella acropodia*. *Centropyxis aculeata*, *C. aculeata grandis*, *C. aculeata minima*, *C. gibba inermis*, and *C. discoidea* were grouped into the *Centropyxis aculeata* type. *Centropyxis platystoma* and *C. elongata* were assigned to the *Centropyxis platystoma* type. *Centropyxis aerophila*, *C. aerophila sphagnicola*, *C. cassis* type, *C. constricta*, *C. constricta minima*, and *C. minuta* were assigned to the *Centropyxis aerophila* type [55]. The conservative approach used in this study means that caution must be exercised when making ecological inferences for some taxa, such as the *Corythion Trinema* type, which is treated as two separate taxa, *Corythion dubium* and *Trinema lineare* [56], as individual taxa within the same group may exhibit different ecological responses.

## 2.4. Statistical Method

Based on the AMS $^{14}\text{C}$  dating data and TA content and concentration data of HT profile, the CONISS program in Tilia 1.7.16 software was used to conduct cluster analyses and classify the assemblage zones of TA. Numerical analyses were conducted on TA taxa that

appeared in a minimum of three samples and had a percentage greater than 1%. A total of 12 TA taxa were chosen for analysis. The square root transformed TA percentage data were analyzed using Canoco 4.5 [57]. Detrended correspondence analysis (DCA) was used to determine whether to use linear or unimodal-based techniques in the subsequent ordination analysis. The first axis had a slope length of 1.858 standard deviation (SD) units, indicating a primarily linear structure and suggesting the use of linear-based principal component analysis (PCA). As a result, PCA was used to analyze the TA assemblages using interspecies correlations and TA percentages.

### 3. Results

#### 3.1. Testate Amoebae Assemblages in the HT Profile

40 families and genera of TA were identified in the 60 samples from the HT profile (Supplementary Table S1); the most abundant TA were *Heleopera petricola/sphagni* (0–7.50%), *Trigonopyxis arcuata* (0–21.14%), *Cyclopyxis arcelloides* (0–10.88%), *Diffflugia lucida* (0–13.95%), *Centropyxis platystoma* type (0.48–25.38%), *Nebela tinctoria* (0–20.88%), *Corythion dubium* (0–7.69%), *Assulina muscorum* (2.02–38.42%), *Euglypha rotunda* (0–20.34%), *Euglypha tuberculata* (0–13.56%), *Heleopera rosea* (0–6.12%), *Nebela lageniformis* (0–6.74%), *Phryganella acropodia* (0–23.53%), *Assulina seminulum* (0–6.29%), and *Hyalosphenia papilio* (0–22.50%). These 15 species represented 80.6% of the total community composition. TA concentrations ranged from  $1.27 \times 10^4$  to  $5.57 \times 10^4$  grains/g. The HT profile's TA diagram was divided into four zones based on TA assemblages and CONISS analysis. Four bio stratigraphic zones were identified using the guidance provided by stratigraphically constrained cluster analysis to facilitate discussion of the major changes in the record.

##### 3.1.1. Zone 1 (Depth Range 60–44 cm): 650–450 cal yr BP

The percentage of *A. muscorum* reached 5.17–26.06%, which was predominant in all the TA assemblages. The percentages of *P. acropodia* and *N. tinctoria* reached 0.98–23.53% and 0–16.43%, respectively. At the depth of 57 cm, *T. arcuata* occurred (21.14%). Total TA concentrations ranged from  $1.62 \times 10^4$  to  $5.57 \times 10^4$  grains/g (Figure 2).

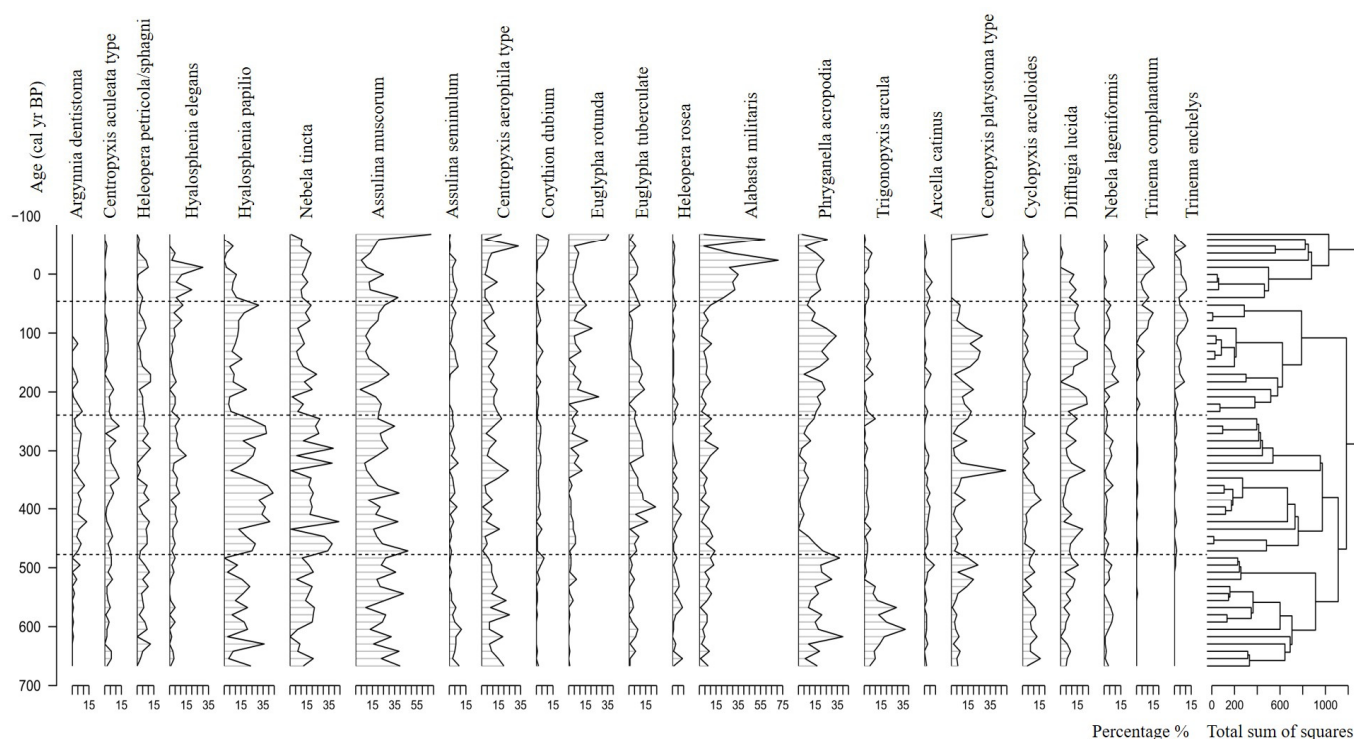


**Figure 2.** Testate amoebae percentage diagram from HT. Zones were identified by CONISS.

3.1.2. Zone 2 (Depth Range 43–25 cm): 400–250 cal yr BP

The species *A. muscorum* and *P. acropodia* were degraded from 400 to 250 cal yr BP, and the percentages were 4.40–18.66% and 0–10%, respectively. During this period, *N. tincta* and *H. papilio* had increased to 0.58–20.88% and 3.49–21.12%, respectively. The species of *A. dentistoma* (0.97–5.91%) and *C. aerophila* type (0.56–13.95%) occurred. TA concentrations dropped down to  $1.27 \times 10^4$ – $5.09 \times 10^4$  grains/g.

3.1.3. Zone 3 (Depth Range 24–12 cm): 200–50 cal yr BP

The proportion of *A. muscorum* (2.02–16.39%) decreased continuously, and *N. tincta* (1.17–13.11%) and *H. papilio* decreased while *P. acropodia* (2.73–20%) increased. In addition, the proportions of *C. aerophila* type and *C. platystoma* type increased to 1.18–7.67% and 1.64–16.47%, respectively. The proportions of *D. lucida* (0–13.95%) and *E. rotunda* (0–15.79%) increased. TA concentrations increased to  $1.49 \times 10^4$ – $5.44 \times 10^4$  grains/g.

3.1.4. Zone 4 (Above 11 cm): 0–50 cal yr BP

Compared with the previous period, the species of *A. militaris* (2.26–40.80%) and *E. rotunda* (2.65–20.34%) were the highest in the whole profile. The proportions of *A. muscorum* (2.87–38.42%) increased while *P. acropodia* (1.69–13.22%) and *H. papilio* (0–15.20%) decreased. The proportions of *D. lucida* (0–8.14%) distinctly dropped, and *H. elegans* (0–17.75%) increased clearly. TA concentrations varied from  $1.39 \times 10^4$  to  $4.69 \times 10^4$  grains/g.

3.2. PCA Analysis

Figure 3 shows the PCA results based on 12 selected TA species and the total number of samples. Axis 1 and axis 2 explain 47.6% of the variation in the selected TA assemblages. The scores of *A. militaris* and *E. rotund* were 1.29 and 0.46, which were at the right end of axis 1. *C. platysoma* type (−0.63), *D. lucida* (−0.49), and *H. papilio* (−1.19) were at the left end of axis 1. On the biplot of the PCA scores on axis 1, the four groups of samples corresponding to the TA combination band can be clearly separated: zone 1 (650–450 cal yr BP) scores ranged from 0.39 to −0.1, zone 2 (400–250 cal yr BP) scores ranged from 0.22 to −1.27, zone 3 (200–50 cal yr BP) scores ranged from 0.46 to −0.83, and zone 4 (0–50 cal yr BP) scores ranged from 2.31 to −0.27.

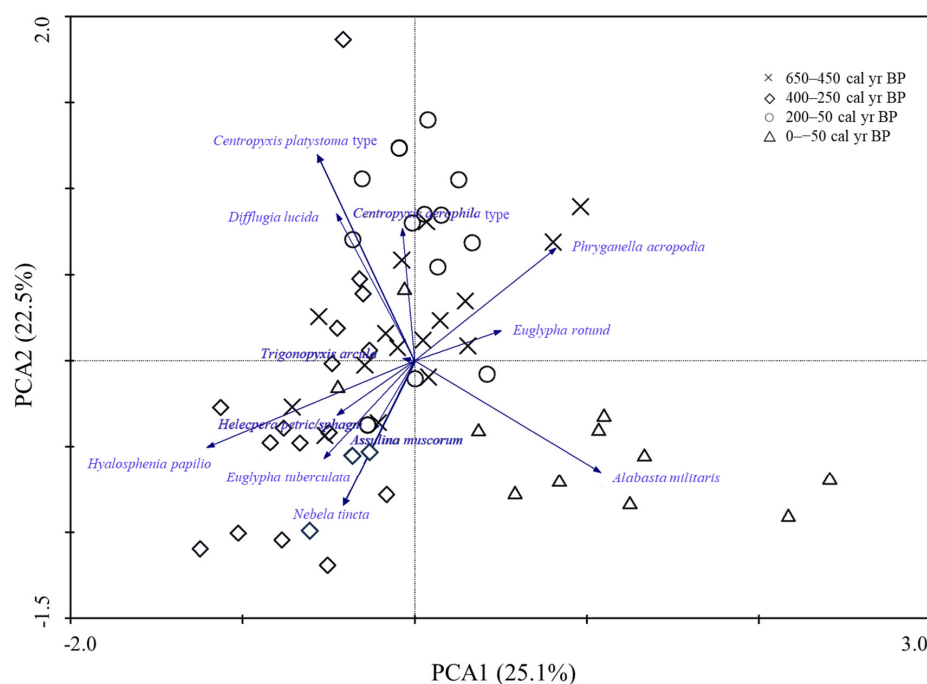


Figure 3. Species ordination plot of PCA analysis with relationship of environmental variables with ordination axis 1 and axis 2.

## 4. Discussion

### 4.1. TA Community Evolution Process of the HT Profile

TA are valuable bioindicators for studying past environmental changes, and their community distributions and abundance are strongly influenced by WTD and humidity [58,59]. By studying the changes of TA communities, we can understand the humidity and WTD status of paleoenvironments and further explore the patterns and mechanisms of environmental changes [34]. Our research results showed that the fossilized TA in the HT peatland revealed diverse and abundant assemblages, dominated by common species with a widely ranging geographical distribution.

At the base of the HT peatland core (650–450 cal yr BP), the dominant taxa are *A. muscorum* and *T. arcuata* (Figure 2). *A. muscorum* and *T. arcuata* are more abundant in boreal peatlands [34,58,59]. In modern ecological research, *A. muscorum* and *T. arcuata* are considered as indicators of drought [29,35,60,61]. In the Tangbei peatland of the Lesser Khingan Mountains, which is close to our study area, Li, Wang, Zhao and Wang [29] found *A. muscorum* with a water table depth (WTD) of 15–45 cm and peat moisture content (water) of 86–91%, and *T. arcuata* with a WTD of 20–50 cm and peat moisture content of 86–90%. As shown in Figure 4, the reconstructed moisture indices in the HT, Tuqiang (TQ), and EASM regions indicated a relatively dry climate during this period [13,38,48]. And the Motianling (MTL) precipitation reconstructed from n-alkanes also found that the climate was in a dry environment during this period [42], so the climate may have influenced the TA species distribution.

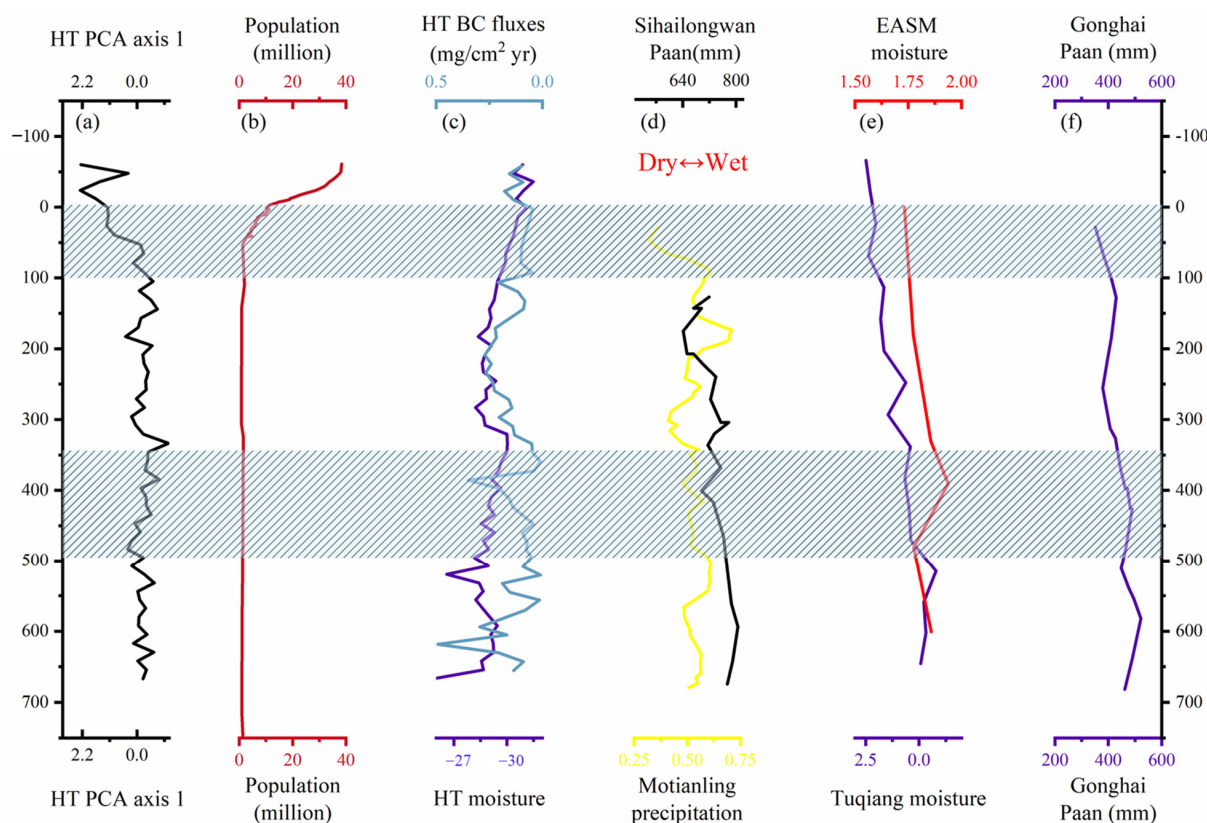


**Figure 4.** (a) Testate amoebae PCA analyses of axis 1 of the HT profile; (b) historical population of Heilongjiang province [62]; (c)  $\delta^{13}\text{C}$ -BC values in the HT region (blue line), BC (black carbon) fluxes in HT (grey line) [38]; (d) precipitation in Sihailongwan Marr Lake reconstructed from pollen data (black line) [46],  $\delta^{13}\text{C}$  record in peat cellulose obtained from the Motianling peatland in the central part of the Greater Khingan mountains (yellow line) [42]; (e) East Asia Summer Monsoon (EASM) moisture (red line) [48], moisture in the Tuqiang peatland reconstructed from pollen data (blue line) [13]; (f) precipitation in Gonghai Lake reconstructed from pollen data [47].

Between 400 and 250 cal yr BP, the percentage of *A. muscorum* and *T. arcula* decreased, while *H. papilio* and *N. tincta* reached high values (Figure 2). *H. papilio* is generally an indicator of wet conditions in peatlands [63–66]. In modern ecological studies, the wide range of optimum water depths for *N. tincta* makes its palaeohydrological reconstruction uncertain. For example, Koenig, Mulot, and Mitchell [67] describe *N. tincta* as an indicator of relatively high water table depth, whereas other studies consider it an indicator of intermediate conditions. Amesbury, Mallon, Charman, Hughes, Booth, Daley, and Garneau [68] emphasize the differences in ecological conditions. The main reason for this is the poor representativeness of modern data concentration species, which may lead to overestimation of palaeohydrological reconstructions. Li, Wang, Zhao, and Wang [29] improved the modern analogue of *N. tincta*, which was placed as an indicator species for moderately wet to dry conditions. Li, Wang, Zhao, and Wang [29] found *H. papilio* at a WTD of 9–30 cm and a peat moisture content of 82–93% in the Tangbei peatland, and *N. tincta* at a WTD of 10–35 cm and a peat moisture content of 87–92%. The  $\delta^{13}\text{C}$ -BC records in the HT peat and the N-alkane records in the MTL peat registered a dry to wet pattern climate at this time [38,42]. The pollen-based reconstruction of moisture and precipitation in the TQ peatland and Sihailongwan (SHLW) Lake showed the same pattern as the HT peat during this period [13,46]. The increased precipitation and moisture can be used to explain the distribution of *H. papilio* and *N. tincta* during 400 and 250 cal yr BP.

During the 150–50 cal yr BP, with the concentrations of *H. papilio* and *N. tincta* declined, the dominant taxon were *P. acropodia*, *A. militaris*, *A. muscorum*, and *D. lucida*. Koenig, Mulot, and Mitchell [67] noted that *P. acropodia* is a species associated with wet to dry peat surface conditions. Li, Wang, Zhao, and Wang [29] found that *D. lucida* in the Tangbei peatland was highly abundant in the intermediate condition at DWT of 15–35 cm and 83–91% peat moisture. *A. muscorum* and *A. militaris* are species related to dry peat surface conditions [69]. Fossil pollen records from the TQ peatlands show that the expansion of birch forests over the last hundred years indicates that the climate of the Greater Khingan Mountains became warmer and drier [70]. The sedimentary record from the MTL peatland and SHLW Maar Lake also shows an increasing pattern in precipitation after 150 cal yr BP [42,46]. The climate change may be the main reason for the increase in these species.

#### 4.2. The Implication of PCA Scores in the HT Peatland

The PCA axis 1 results have explained 25.1% of the variation in selected TA assemblages. Several TA species commonly associated with wet and moderate habitats, such as *H. papilio*, *N. tincta*, *C. aerophila* type, and *E. tuberculata* were on the left side of axis 1. For instance, *H. papilio* had the lowest score (−1.19) on axis 1 and it was confirmed to be distributed in a high WTD and acidic environment [29]. This suggests that the smaller the species and sample scores for PCA axis 1, the wetter the environment is indicated. TA dry indicators such as *A. militaris*, *E. rotund*, and *P. acropodia* were on the right side of axis. These species had higher scores in axis 1, and they have stable conditions distributed in drier and acid environment. Nevertheless, the other common TA dry indicators such as *A. muscorum* and *T. arcula* were on the middle position of axis 1. This may be because dry species generally have broader tolerances than wet species [68,69]. Thus, the results of species and sample scores on axis 1 can be used as indirect indicators of palaeohydrological variation in the HT peatland.

Prior to 500 cal yr BP, PCA axis 1 values in the HT peat core fluctuated slightly (Figure 5), with close agreement with the reconstructed moisture from pollen in the TQ peatland and the EASM moisture index [13,71]. The mean annual precipitation reconstructed from GH Lake showed the same pattern as axis 1 [47]. And the MTL precipitation index reconstructed from n-alkanes also found that the climate was in a dry environment during this period [42]. During 500–350 cal yr BP, the scores of HT axis 1 decreased, which indicates a wetter climate. The reconstructed moisture from  $\delta^{13}\text{C}$ -BC and pollen in the HT and TQ peatlands and EASM moisture index showed a similar pattern to axis 1 [13,38,48]. The mean annual precipitation reconstruction of SHLW Marr Lake and GH Lake showed a

pattern of high precipitation during this period [46,47]. And the MTL precipitation index reconstructed from n-alkanes also found that the climate was in a dry and cold environment during this period [42]. During the interval from 300 to 100 cal yr BP, the higher value of PCA axis 1 scores reflects a drier environment, and the  $\delta^{13}\text{C-BC}$  regional environmental reconstruction in the HT peatland shows a dry and cold climate during the same period [38]. The precipitation index of n-alkanes in the MTL peatland are similar to those of PCA axis 1, indicating that this period was dry [42]. The pollen-based moisture index and temperature index in the TQ peatland and SHLW Marr Lake also indicate a colder and drier climate during the same period [13,46]. The EASM moisture also showed a decreased pattern of precipitation [71]. The BC fluxes of HT peatlands showed a higher frequency of forest fire events caused by a drier climate [38]. The climate was colder and drier at that time, likely related to the Little Ice Age (1550–1850 AD) [72]. Since 50 cal yr BP, the scores of PCA axis 1 have shown a drier climate. The increasing historical population in the Heilongjiang Province has led to an increase in drying due to human activities [62]. The sedimentary records of MTL and TQ peatlands also show an increasing pattern in temperature and precipitation after the Little Ice Age. The reconstruction of mean annual precipitation from SHLW Maar Lake showed lower precipitation levels [46]. The different proxies showed that HT is becoming increasingly dry as a result of climate change and human activity. In the future, we will establish the transfer function between TA and environmental factors in this region, and apply it to reconstructing paleoclimate and paleoenvironment.

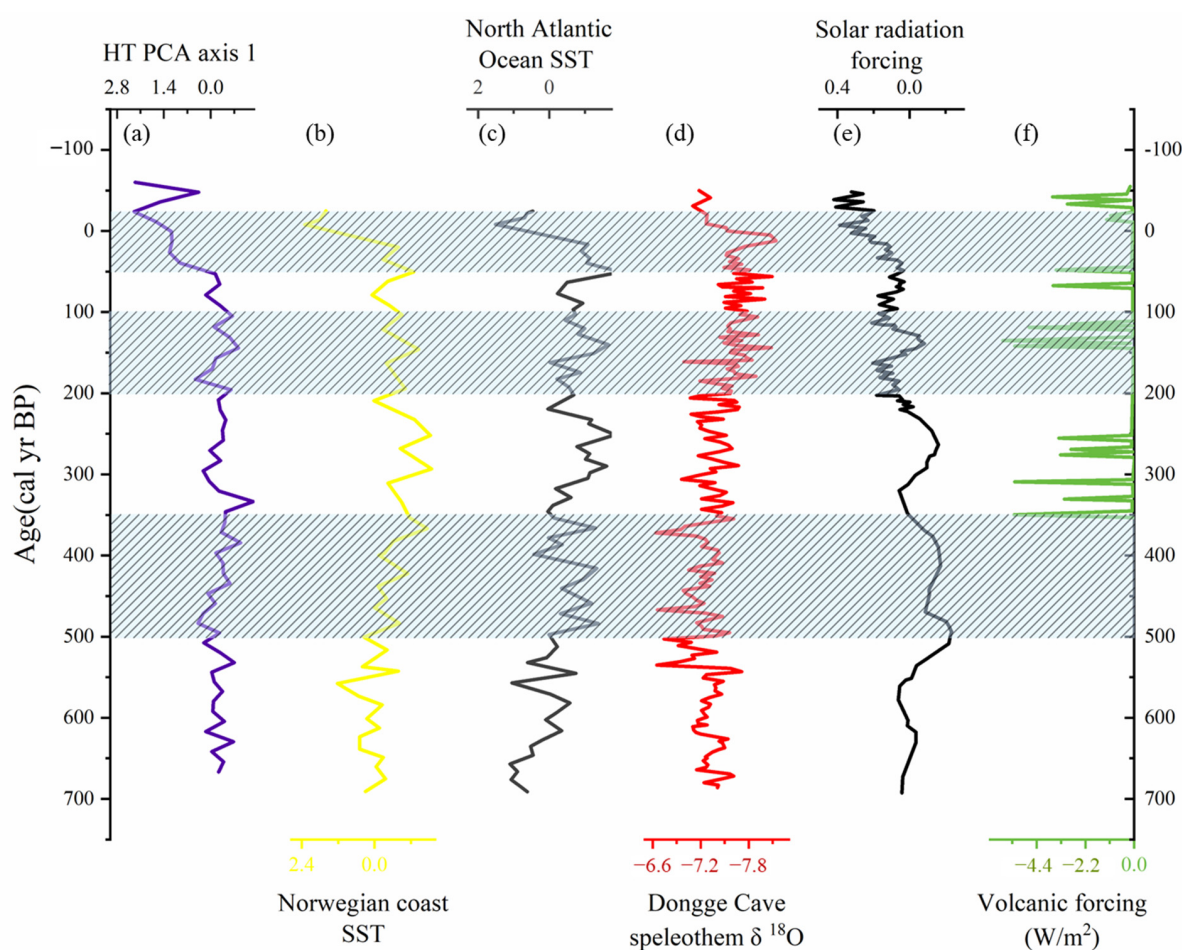


**Figure 5.** Comparison of PCA axis 1 score curves from the HT peatland with other selected proxy records. (a) Testate amoebae PCA analyses of axis 1 of the HT profile; (b) sea surface temperature (SST) from the Norwegian coast [73]; (c) SST from the North Atlantic [73]; (d) Dongge Cave speleothem  $\delta^{18}\text{O}$  records [74]; (e) solar radiation forcing in the tropical Pacific [75]; (f) volcanic forcing in the tropical Pacific [75].

#### 4.3. Possible Forcing Mechanisms of Climate at the HT Peatland

Solar radiative forcing and volcanic forcing are the two main factors influencing global climate change [75]. The impact of these two factors on the climate characteristics of HT in the Greater Khingan Mountains over the past millennium can be assessed using model-reconstructed tropical Pacific solar radiative forcing and volcanic forcing. The HT peatland is located at the northernmost end of the EASM, and the strengthening and weakening of the EASM has an important influence on precipitation in the study area [13]. Precipitation can directly reflect the intensity of the EASM, and the tropical and subtropical Pacific will transport more/less water vapor to make the East Asian monsoon circulation stronger/weaker, resulting in an increase or decrease in precipitation [75]. The  $\delta^{18}\text{O}$  values in the Dongge Cave and North Atlantic Sea surface temperatures (SST) reflect the historical changes in the East Asian monsoon and wet zone over the past millennium [73,74]. By perturbing atmospheric circulation and water vapor transport, ocean thermal states, which are closely linked to solar activity, can lead to arid and humid climates. Ocean–atmosphere interactions play an important role in driving the monsoon and controlling precipitation [76].

Historical variations in SST in the northeastern Atlantic, influenced by solar radiative forcing, may directly affect winter temperatures in the western region [77]. Decreases in solar radiative forcing result in low winter temperatures over northern hemisphere continents [78]. Between 650 and 450 cal yr BP, the western tropical Pacific experienced higher SST, which intensified the monsoon and brought more rainfall to the region being studied [73]. Meanwhile, records of Norwegian coastal SST, North Atlantic SST, and solar radiation also showed stronger EASM intensity during this period [73]. The climate in HT was primarily influenced by the EASM, which was connected to interactions between the ocean and atmosphere. During the period from 350 to 100 cal yr BP, the value of PCA axis 1 indicates a dry climate in HT. The decrease in the values of the SST of the Norwegian coast and the SST of the North Atlantic Ocean supports our TA-based conclusion of the cold and dry climate associated with the Little Ice Age [73]. The speleothem  $\delta^{18}\text{O}$  records in Dongge Cave showed a feeble EASM strength [74].

Since 50 cal yr BP the climate has tended to be drier, supported by increasing values of SST along the Norwegian coast and SST in the North Atlantic [73]. However, as the solar radiative forcing became stronger, the climatic characteristics of the HT bog became warmer and drier. We speculate that with the dramatic increase in population, modern climate warming and decreased precipitation are more influenced by anthropogenic disturbances. Simulations of temperature changes due to solar activity suggest that there may be simple mechanisms that can help explain the observed data [74,75]. High irradiance increases surface air temperature, with the strongest correlation between solar activity and temperature change in the tropics and subtropics. However, the greatest change occurs at high latitudes, resulting in a smaller temperature difference between the equator and poles when solar irradiance is high. These may lead to weaker North Atlantic trade winds during solar maxima and an intensified monsoon in Oman due to a greater temperature difference between land and ocean [74]. The decrease in humidity in HT over the past millennium correlates with other records from northern low latitudes and is due to a decrease in summer insolation caused by changes in Earth's orbit, which affects precipitation patterns. The centennial and multidecadal events in the HT record can be partly attributed to changes in solar activity. There are also correlations between the HT and North Atlantic climates, including the Norwegian coastal record, due to solar activity affecting both regions. Changes in ocean circulation in the North Atlantic may also have triggered changes in HT, as seen in the 350 cal yr BP event. Climate changes in HT over the past millennium result from a combination of factors, including changes in insolation, solar activity, and oceanic and atmospheric circulation.

## 5. Conclusions

We inferred a ~800-year record of environmental change in the Hongtu (HT) peatland of the Greater Khingan Mountains. A total of 40 species of TA were identified in the HT peat core. The paleoclimatic record based on TA records of the HT peatland concluded that the history of protists and climate changes during the last millennium showed strong similarities with other paleoclimatic proxy records in the East Summer Monsoon region. The results of PCA axis 1 showed an HT climate with a wet to dry pattern during the last millennium. The climate of the northern part of the Greater Khingan Mountains was mainly controlled by the EASM, which was related to ocean–atmosphere interactions in the tropical Pacific, and was associated with changes in SST in the North Atlantic Ocean and solar radiative forcing. Therefore, precipitation and humidity may decrease in the Greater Khingan Mountains, leading to potential ecological changes. Additionally, a potential weakening or shift of the EASM could further exacerbate climate changes in the Greater Khingan Mountains. As a result, ecological conservation and climate change adaptation measures in the region should consider these potential impacts and develop appropriate responses accordingly.

**Supplementary Materials:** The following supporting information can be downloaded at: <https://www.mdpi.com/article/10.3390/atmos15030314/s1>, Table S1: 60 samples from the HT profile.

**Author Contributions:** X.L., G.W. and C.G. conceived and conducted the experiments, X.L. designed and carried out the data analysis, and co-wrote the paper together with C.G., D.H. and J.C. All co-authors were involved in sample preparation and provided helpful feedback for this paper. All authors have read and agreed to the published version of the manuscript.

**Funding:** Financial support was provided by the National Natural Science Foundation of China (Nos. 42330509, 42301120, 42101108, and 42171103), the Young Scientist Group Project of the Northeast Institute of Geography and Agroecology, Chinese Academy of Sciences (2022QNXX01), and the Youth Innovation Promotion Association CAS (No. 2020235).

**Institutional Review Board Statement:** Not applicable.

**Informed Consent Statement:** Not applicable.

**Data Availability Statement:** All data will be available upon reasonable request.

**Conflicts of Interest:** The authors declare that they have no known competing financial interests or personal relationships that could have appeared to influence the work reported in this paper.

## References

1. An, Z.; Colman, S.M.; Zhou, W.; Li, X.; Brown, E.T.; Jull, A.J.; Cai, Y.; Huang, Y.; Lu, X.; Chang, H.; et al. Interplay between the Westerlies and Asian monsoon recorded in Lake Qinghai sediments since 32 ka. *Sci. Rep.* **2012**, *2*, 619. [[CrossRef](#)]
2. Ji, J.; Shen, J.; Balsam, W.; Chen, J.; Liu, L.; Liu, X. Asian monsoon oscillations in the northeastern Qinghai–Tibet Plateau since the late glacial as interpreted from visible reflectance of Qinghai Lake sediments. *Earth Planet. Sci. Lett.* **2005**, *233*, 61–70. [[CrossRef](#)]
3. Turner, A.G.; Annamalai, H. Climate change and the South Asian summer monsoon. *Nat. Clim. Change* **2012**, *2*, 587–595. [[CrossRef](#)]
4. Wen, R.; Xiao, J.; Chang, Z.; Zhai, D.; Xu, Q.; Li, Y.; Itoh, S. Holocene precipitation and temperature variations in the East Asian monsoonal margin from pollen data from Hulun Lake in northeastern Inner Mongolia, China. *Boreas* **2010**, *39*, 262–272. [[CrossRef](#)]
5. Charman, D.J.; Hohl, V.; Blundell, A.; Mitchell, F.; Newberry, J.; Oksanen, P. A 1000-year reconstruction of summer precipitation from Ireland: Calibration of a peat-based palaeoclimate record. *Quat. Int.* **2012**, *268*, 87–97. [[CrossRef](#)]
6. Jones, P.D.; Briffa, K.R.; Osborn, T.J.; Lough, J.M.; van Ommen, T.D.; Vinther, B.M.; Luterbacher, J.; Wahl, E.R.; Zwiiers, F.W.; Mann, M.E.; et al. High-resolution palaeoclimatology of the last millennium: A review of current status and future prospects. *Holocene* **2009**, *19*, 3–49. [[CrossRef](#)]
7. Guo, Y.; Zhao, Z.; Zhu, F.; Li, X. Climate change may cause distribution area loss for tree species in southern China. *For. Ecol. Manag.* **2022**, *511*, 120134. [[CrossRef](#)]
8. Liu, J.; Zhang, Q.; Deng, X.; Chen, C. Quantitative analysis the influences of climate change and human activities on hydrological processes in Poyang Basin. *J. Lake Sci.* **2016**, *28*, 432–443.
9. Dang, Y.; He, H.; Zhao, D.; Sunde, M.; Du, H. Quantifying the Relative Importance of Climate Change and Human Activities on Selected Wetland Ecosystems in China. *Sustainability* **2020**, *12*, 912. [[CrossRef](#)]
10. Li, W.; Zhao, S.; Chen, Y.; Wang, Q.; Ai, W. State of China’s Climate in 2020. *Atmos. Ocean. Sci. Lett.* **2021**, *14*, 100048. [[CrossRef](#)]

11. Choi, G.; Collins, D.; Ren, G.; Trewin, B.; Baldi, M.; Fukuda, Y.; Afzaal, M.; Pianmana, T.; Gomboluudev, P.; Huong, P.T.T.; et al. Changes in means and extreme events of temperature and precipitation in the Asia-Pacific Network region, 1955–2007. *Int. J. Climatol.* **2009**, *29*, 1906–1925. [[CrossRef](#)]
12. Zhao, K.; Wang, Y.; Edwards, R.L.; Cheng, H.; Liu, D.; Kong, X. A high-resolved record of the Asian Summer Monsoon from Dongge Cave, China for the past 1200 years. *Quat. Sci. Rev.* **2015**, *122*, 250–257. [[CrossRef](#)]
13. Han, D.; Gao, C.; Yu, Z.; Yu, X.; Li, Y.; Cong, J.; Wang, G. Late Holocene vegetation and climate changes in the Great Hinggan Mountains, northeast China. *Quat. Int.* **2019**, *532*, 138–145. [[CrossRef](#)]
14. Xiao, J.; Fan, J.; Zhai, D.; Wen, R.; Qin, X. Testing the model for linking grain-size component to lake level status of modern clastic lakes. *Quat. Int.* **2015**, *355*, 34–43. [[CrossRef](#)]
15. Bysouth, D.; Finkelstein, S.A. Linking testate amoeba assemblages to paleohydrology and ecosystem function in Holocene peat records from the Hudson Bay Lowlands, Ontario, Canada. *Holocene* **2020**, *31*, 457–468. [[CrossRef](#)]
16. Łuców, D.; Küttim, M.; Słowiński, M.; Kołaczek, P.; Karpińska-Kołaczek, M.; Küttim, L.; Salme, M.; Lamentowicz, M. Searching for an ecological baseline: Long-term ecology of a post-extraction restored bog in Northern Estonia. *Quat. Int.* **2021**, *607*, 65–78. [[CrossRef](#)]
17. Mikhailova, A.B.; Grenaderova, A.V.; Kurina, I.V.; Shumilovskikh, L.S.; Stojko, T.G. Holocene vegetation and hydroclimate changes in the Kansk forest steppe, Yenisei River Basin, East Siberia. *Boreas* **2021**, *50*, 948–966. [[CrossRef](#)]
18. Ndayishimiye, J.C.; Lin, T.; Nyirabuhoro, P.; Zhang, G.; Zhang, W.; Mazei, Y.; Ganjidoust, H.; Yang, J. Decade-scale change in testate amoebae community primarily driven by anthropogenic disturbance than natural change in a large subtropical reservoir. *Sci. Total Environ.* **2021**, *784*, 147026. [[CrossRef](#)]
19. Nova, C.C.; Rocha, A.M.; Branco, C.W.C.; Bozelli, R.L. New insights on the relation between zooplankton and humic substances in tropical freshwater ecosystems. *An. Acad. Bras. Ciências* **2021**, *93*, e20190409. [[CrossRef](#)] [[PubMed](#)]
20. Charman, D.J. Biostratigraphic and palaeoenvironmental applications of testate amoebae. *Quat. Sci. Rev.* **2001**, *20*, 1753–1764. [[CrossRef](#)]
21. Mitchell, E.A.D.; Charman, D.J.; Warner, B.G. Testate amoebae analysis in ecological and paleoecological studies of wetlands: Past, present and future. *Biodivers. Conserv.* **2007**, *17*, 2115–2137. [[CrossRef](#)]
22. Booth, R.K. Testate amoebae as paleoindicators of surface-moisture changes on Michigan peatlands: Modern ecology and hydrological calibration. *J. Paleolimnol.* **2002**, *28*, 329–348. [[CrossRef](#)]
23. Qin, Y.; Xie, S.; Smith, H.G.; Swindles, G.T.; Gu, Y. Diversity, distribution and biogeography of testate amoebae in China: Implications for ecological studies in Asia. *Eur. J. Protistol.* **2011**, *47*, 1–9. [[CrossRef](#)]
24. Qin, Y.; Zhang, L.; Swindles, G.T.; Yang, H.; Gu, Y.; Qi, S. A ~40-year paleoenvironmental record from the Swan Oxbow, Yangtze River, China, inferred from testate amoebae and sedimentary pigments. *J. Paleolimnol.* **2021**, *66*, 29–40. [[CrossRef](#)]
25. Swindles, G.T.; Morris, P.J.; Mullan, D.J.; Payne, R.J.; Roland, T.P.; Amesbury, M.J.; Lamentowicz, M.; Turner, T.E.; Gallego-Sala, A.; Sim, T.; et al. Widespread drying of European peatlands in recent centuries. *Nat. Geosci.* **2019**, *12*, 922–928. [[CrossRef](#)]
26. Booth, R.K.; Lamentowicz, M.; Charman, D.J. Preparation and analysis of testate amoebae in peatland palaeoenvironmental studies. *Mires. Peat.* **2010**, *7*, 1–7.
27. Mazei, Y.A.; Tsyganov, A.N.; Esaulov, A.S.; Tychkov, A.Y.; Payne, R.J. What is the optimum sample size for the study of peatland testate amoeba assemblages? *Eur. J. Protistol.* **2017**, *61*, 85–91. [[CrossRef](#)]
28. Marcisz, K.; Jassey, V.E.J.; Kosakyan, A.; Krashevskaya, V.; Lahr, D.J.G.; Lara, E.; Lamentowicz, L.; Lamentowicz, M.; Macumber, A.; Mazei, Y.; et al. Testate Amoeba Functional Traits and Their Use in Paleoecology. *Front. Ecol. Evol.* **2020**, *8*, 575966. [[CrossRef](#)]
29. Li, H.; Wang, S.; Zhao, H.; Wang, M. A testate amoebae transfer function from Sphagnum-dominated peatlands in the Lesser Khingan Mountains, NE China. *J. Paleolimnol.* **2015**, *54*, 189–203. [[CrossRef](#)]
30. Stastney, P.; Black, S. Bog Microtopography and the Climatic Sensitivity of Testate Amoeba Communities: Implications for Transfer Function-Based Paleo-Water Table Reconstructions. *Microb. Ecol.* **2020**, *80*, 309–321. [[CrossRef](#)]
31. Payne, R.J.; Telford, R.J.; Blackford, J.J.; Blundell, A.; Booth, R.K.; Charman, D.J.; Lamentowicz, L.; Lamentowicz, M.; Mitchell, E.A.D.; Potts, G.; et al. Testing peatland testate amoeba transfer functions: Appropriate methods for clustered training-sets. *Holocene* **2011**, *22*, 819–825. [[CrossRef](#)]
32. Turner, T.E.; Swindles, G.T.; Charman, D.J.; Blundell, A. Comparing regional and supra-regional transfer functions for palaeohydrological reconstruction from Holocene peatlands. *Palaeogeogr. Palaeoclimatol. Palaeoecol.* **2013**, *369*, 395–408. [[CrossRef](#)]
33. Chen, J.; Lv, F.; Huang, X.; Birks, H.J.B.; Telford, R.J.; Zhang, S.; Xu, Q.; Zhao, Y.; Wang, H.; Zhou, A.; et al. A novel procedure for pollen-based quantitative paleoclimate reconstructions and its application in China. *Sci. China Earth Sci.* **2017**, *60*, 2059–2066. [[CrossRef](#)]
34. Halaś, A.; Lamentowicz, M.; Łuców, D.; Słowiński, M. Developing a new testate amoeba hydrological transfer function for permafrost peatlands of NW Siberia. *Quat. Sci. Rev.* **2023**, *308*, 108067. [[CrossRef](#)]
35. Qin, Y.; Li, H.; Mazei, Y.; Kurina, I.; Swindles, G.T.; Bobrov, A.; Tsyganov, A.N.; Gu, Y.; Huang, X.; Xue, J.; et al. Developing a continental-scale testate amoeba hydrological transfer function for Asian peatlands. *Quat. Sci. Rev.* **2021**, *258*, 106868. [[CrossRef](#)]
36. Amesbury, M.J.; Swindles, G.T.; Bobrov, A.; Charman, D.J.; Holden, J.; Lamentowicz, M.; Mallon, G.; Mazei, Y.; Mitchell, E.A.D.; Payne, R.J.; et al. Development of a new pan-European testate amoeba transfer function for reconstructing peatland palaeohydrology. *Quat. Sci. Rev.* **2016**, *152*, 132–151. [[CrossRef](#)]

37. Gatis, N.; Benaud, P.; Anderson, K.; Ashe, J.; Grand-Clement, E.; Luscombe, D.J.; Puttock, A.; Brazier, R.E. Peatland restoration increases water storage and attenuates downstream stormflow but does not guarantee an immediate reversal of long-term ecohydrological degradation. *Sci. Rep.* **2023**, *13*, 15865. [CrossRef]
38. Gao, C.; He, J.; Zhang, Y.; Cong, J.; Han, D.; Wang, G. Fire history and climate characteristics during the last millennium of the Great Hinggan Mountains at the monsoon margin in northeastern China. *Glob. Planet. Change* **2018**, *162*, 313–320. [CrossRef]
39. Rahimi, J.; Laux, P.; Khalili, A. Assessment of climate change over Iran: CMIP5 results and their presentation in terms of Köppen–Geiger climate zones. *Theor. Appl. Climatol.* **2020**, *141*, 183–199. [CrossRef]
40. Valjarević, A.; Milanović, M.; Gulpepe, I.; Filipović, D.; Lukić, T. Updated Trewartha climate classification with four climate change scenarios. *Geogr. J.* **2022**, *188*, 506–517. [CrossRef]
41. Gao, C.; He, J.; Cong, J.; Zhang, S.; Wang, G. Impact of forest fires generated black carbon deposition fluxes in Great Hinggan Mountains (China). *Land Degrad. Dev.* **2018**, *29*, 2073–2081. [CrossRef]
42. Zhang, Y.; Liu, X.; Lin, Q.; Gao, C.; Wang, J.; Wang, G. Vegetation and climate change over the past 800 years in the monsoon margin of northeastern China reconstructed from n-alkanes from the Great Hinggan Mountain ombrotrophic peat bog. *Org. Geochem.* **2014**, *76*, 128–135. [CrossRef]
43. Cong, J.; Gao, C.; Ji, S.; Li, X.; Han, D.; Wang, G. Changes in organic matter properties and carbon chemical stability in surface soils associated with changing vegetation communities in permafrost peatlands. *Biogeochemistry* **2023**, *163*, 139–153. [CrossRef]
44. CMA. Introduce of Mohe. 2016. Available online: <http://www.weather.com.cn/cityintro/101050703.html> (accessed on 19 November 2016).
45. Han, D.; Gao, C.; Liu, H.; Yu, X.; Li, Y.; Cong, J.; Wang, G. Vegetation dynamics and its response to climate change during the past 2000 years along the Amur River Basin, Northeast China. *Ecol. Indic.* **2020**, *117*, 106577. [CrossRef]
46. Stebich, M.; Rehfeld, K.; Schlütz, F.; Tarasov, P.E.; Liu, J.; Mingram, J. Holocene vegetation and climate dynamics of NE China based on the pollen record from Sihailongwan Maar Lake. *Quat. Sci. Rev.* **2015**, *124*, 275–289. [CrossRef]
47. Chen, F.; Xu, Q.; Chen, J.; Birks, H.J.; Liu, J.; Zhang, S.; Jin, L.; An, C.; Telford, R.J.; Cao, X.; et al. East Asian summer monsoon precipitation variability since the last deglaciation. *Sci. Rep.* **2015**, *5*, 11186. [CrossRef] [PubMed]
48. Chen, F.; Yu, Z.; Yang, M.; Ito, E.; Wang, S.; Madsen, D.B.; Huang, X.; Zhao, Y.; Sato, T.; Birks, J.B.H.; et al. Holocene moisture evolution in arid central Asia and its out-of-phase relationship with Asian monsoon history. *Quat. Sci. Rev.* **2008**, *27*, 351–364. [CrossRef]
49. Zhou, W.; Lu, X.; Wu, Z.; Deng, L.; Jull, A.J.T.; Beck, D.D. Peat record reflecting Holocene climatic change in the Zoigê Plateau and AMS radiocarbon dating. *Chin. Sci. Bull.* **2002**, *47*, 66–70. [CrossRef]
50. Stuiver, M.; Reimer, P.J.; Reimer, R.W. CALIB 7.1. 2016. Available online: <http://Calib.org> (accessed on 13 November 2016).
51. Charman, D.J.; Hendon, D.; Woodland, W.A. The identification of testate amoebae (Protozoa: Rhizopoda) in peats. *Quat. Sci. Rev.* **2004**, *23*, 1867–1870.
52. Zheng, X.; Harper, J.B.; Hope, G.; Mooney, S.D. A new preparation method for testate amoebae in minerogenic sediments. *Mires. Peat.* **2019**, *24*, 1–12.
53. Sim, T.G.; Swindles, G.T.; Morris, P.J.; Baird, A.J.; Charman, D.J.; Amesbury, M.J.; Beilman, D.; Channon, A.; Gallego-Sala, A.V. Ecology of peatland testate amoebae in Svalbard and the development of transfer functions for reconstructing past water-table depth and pH. *Ecol. Indic.* **2021**, *131*, 108122. [CrossRef]
54. Sim, T.G.; Swindles, G.T.; Morris, P.J.; Baird, A.J.; Cooper, C.L.; Gallego-Sala, A.V.; Charman, D.J.; Roland, T.P.; Borke, W.; Mullan, D.J.; et al. Divergent responses of permafrost peatlands to recent climate change. *Environ. Res. Lett.* **2021**, *16*, 034001. [CrossRef]
55. Dumack, K.; Görzen, D.; González-Miguéns, R.; Siemensma, F.; Lahr, D.J.G.; Lara, E.; Bonkowski, M. Molecular investigation of *Phryganella acropodia* Hertwig et Lesser, 1874 (Arcellinida, Amoebozoa). *Eur. J. Protistol.* **2020**, *75*, 125707. [CrossRef]
56. Charman, D.J.; Hendon, D.; Woodland, A.A. *The Identification of Testate Amoebae (Protozoa: Rhizopoda) from British Oligotrophic Peats*; Quaternary Research Association Technical Guide Series; Cambridge University Press: Cambridge, UK, 2000.
57. Leps, J.; Smilauer, P. *Multivariate Analysis of Ecological Data using CANOCO: Using the Canoco for Windows 4.5 package*. In *Multivariate Analysis of Ecological Data Using CANOCO*; Cambridge University Press: Cambridge, UK, 2003; pp. 43–59.
58. Tsyganov, A.N.; Chertoprud, E.S.; Mazei, N.G.; Esaulov, A.S.; Sadchikov, I.P.; Mazei, Y.A. The Effects of Vegetation and the Environment on Testate Amoeba Assemblages in Sphagnum Peatlands in the Northern Caucasus Mountains. *Diversity* **2023**, *15*, 258. [CrossRef]
59. Seppey, C.V.W.; Lara, E.; Broennimann, O.; Guisan, A.; Malard, L.; Singer, D.; Yashiro, E.; Fournier, B. Landscape structure is a key driver of soil protist diversity in meadows in the Swiss Alps. *Landsc. Ecol.* **2023**, *38*, 949–965. [CrossRef]
60. Diaconu, A.-C.; Tóth, M.; Lamentowicz, M.; Heiri, O.; Kuske, E.; Tanțău, I.; Panait, A.-M.; Braun, M.; Feurdean, A. How warm? How wet? Hydroclimate reconstruction of the past 7500 years in northern Carpathians, Romania. *Palaeogeogr. Palaeoclimatol. Palaeoecol.* **2017**, *482*, 1–12. [CrossRef]
61. Warner, B.G.; Charman, D.J. Holocene changes on a peatland in northwestern Ontario interpreted from testate amoebae (Protozoa) analysis. *Boreas* **1994**, *23*, 270–279. [CrossRef]
62. Cong, J.; Gao, C.; Zhang, Y.; Zhang, S.; He, J.; Wang, G. Dating the period when intensive anthropogenic activity began to influence the Sanjiang Plain, Northeast China. *Sci. Rep.* **2016**, *6*, 22153. [CrossRef] [PubMed]
63. Lamentowicz, Ł.; Gabka, M.; Lamentowicz, M. Species composition of testate amoebae (Protists) and environmental parameters in a Sphagnum peatland. *Pol. J. Ecol.* **2007**, *55*, 749–759.

64. Magnan, G.; Lacourse, T.; Garneau, M. A comparison of Holocene testate amoeba assemblages and paleohydrological records from pollen slides and wet-sieved peat. *Holocene* **2020**, *31*, 73–82. [[CrossRef](#)]
65. Marcisz, K.; Colombaroli, D.; Jassey, V.E.; Tinner, W.; Kolaczek, P.; Galka, M.; Karpinska-Kolaczek, M.; Slowinski, M.; Lamentowicz, M. A novel testate amoebae trait-based approach to infer environmental disturbance in Sphagnum peatlands. *Sci. Rep.* **2016**, *6*, 33907. [[CrossRef](#)]
66. Mazei, Y.A.; Trulova, A.; Mazei, N.G.; Payne, R.J.; Tsyganov, A.N. Contributions of temporal and spatial variation to the diversity of soil-dwelling testate amoeba assemblages in a swampy forest. *Pedobiologia* **2020**, *81*, 150660. [[CrossRef](#)]
67. Koenig, I.; Mulot, M.; Mitchell, E.A.D. Taxonomic and functional traits responses of Sphagnum peatland testate amoebae to experimentally manipulated water table. *Ecol. Indic.* **2018**, *85*, 342–351. [[CrossRef](#)]
68. Amesbury, M.J.; Mallon, G.; Charman, D.J.; Hughes, P.D.M.; Booth, R.K.; Daley, T.J.; Garneau, M. Statistical testing of a new testate amoeba-based transfer function for water-table depth reconstruction on ombrotrophic peatlands in north-eastern Canada and Maine, United States. *J. Quat. Sci.* **2013**, *28*, 27–39. [[CrossRef](#)]
69. Lamentowicz, L.; Lamentowicz, M.; Gabka, M. Testate amoebae ecology and a local transfer function from a peatland in western Poland. *Wetlands* **2008**, *28*, 164–175. [[CrossRef](#)]
70. Han, D.; Gao, C.; Liu, H.; Li, Y.; Cong, J.; Yu, X.; Wang, G. Anthropogenic and climatic-driven peatland degradation during the past 150 years in the Greater Khingan Mountains, NE China. *Land Degrad. Dev.* **2021**, *32*, 4845–4857. [[CrossRef](#)]
71. Chen, F.-H.; Chen, J.-H.; Holmes, J.; Boomer, I.; Austin, P.; Gates, J.B.; Wang, N.-L.; Brooks, S.J.; Zhang, J.-W. Moisture changes over the last millennium in arid central Asia: A review, synthesis and comparison with monsoon region. *Quat. Sci. Rev.* **2010**, *29*, 1055–1068. [[CrossRef](#)]
72. Jin, H.; Jin, X.; He, R.; Luo, D.; Chang, X.; Wang, S.; Marchenko, S.S.; Yang, S.; Yi, C.; Li, S.; et al. Evolution of permafrost in China during the last 20 ka. *Sci. China Earth Sci.* **2018**, *62*, 1207–1223. [[CrossRef](#)]
73. Cunningham, L.K.; Austin, W.E.N.; Knudsen, K.L.; Eiriksson, J.; Scourse, J.D.; Wanamaker, A.D.; Butler, P.G.; Cage, A.G.; Richter, T.; Husum, K.; et al. Reconstructions of surface ocean conditions from the northeast Atlantic and Nordic seas during the last millennium. *Holocene* **2013**, *23*, 921–935. [[CrossRef](#)]
74. Wang, Y.; Cheng, H.; Edwards, R.L.; He, Y.; Kong, X.; An, Z.; Wu, J.; Kelly, M.J.; Dykoski, C.A.; Li, X. The Holocene Asian monsoon: Links to solar changes and North Atlantic climate. *Science* **2005**, *308*, 854–857. [[CrossRef](#)] [[PubMed](#)]
75. Mann, M.E.; Cane, M.A.; Zebiak, S.E.; Clement, A. Volcanic and solar forcing of the tropical Pacific over the past 1000 years. *J. Clim.* **2005**, *18*, 447–456. [[CrossRef](#)]
76. Schmidt, M.W.; Chang, P.; Parker, A.O.; Ji, L.; He, F. Deglacial Tropical Atlantic subsurface warming links ocean circulation variability to the West African Monsoon. *Sci. Rep.* **2017**, *7*, 15390. [[CrossRef](#)] [[PubMed](#)]
77. Yang, L.; Wu, B. Interdecadal variations of the East Asian winter surface air temperature and possible causes. *Chin. Sci. Bull.* **2013**, *58*, 3969–3977. [[CrossRef](#)]
78. Shindell, D.T.; Schmidt, G.A.; Mann, M.E.; Rind, D.; Waple, A. Solar forcing of regional climate change during the Maunder Minimum. *Science* **2001**, *294*, 2149–2152. [[CrossRef](#)]

**Disclaimer/Publisher’s Note:** The statements, opinions and data contained in all publications are solely those of the individual author(s) and contributor(s) and not of MDPI and/or the editor(s). MDPI and/or the editor(s) disclaim responsibility for any injury to people or property resulting from any ideas, methods, instructions or products referred to in the content.